Simulation of a Nested Channel Hall Thruster

IEPC-2015-250／ISTS-2015-b-250

Presented at Joint Conference of 30th International Symposium on Space Technology and Science,
34th International Electric Propulsion Conference and 6th Nano-satellite Symposium
Hyogo-Kobe, Japan
July 4–10, 2015

Horatiu C. Dragnea* and Iain D. Boyd†
University of Michigan, Ann Arbor, MI, 48109, U.S.A.

Nested channel Hall thrusters are a recent development, and the mechanism of channel interaction is a topic that has to be explored further in order to optimize the technology. The present work represents a first step in simulating a 10 kW class dual channel device, and is focused on the inner channel independent operation. The state of the art 2D axisymmetric hybrid-PIC code HPHall is used. This computational tool is evaluated by observing the effects of charge exchange collisions, number of particles, mobility parameters and electron temperature anisotropy ratio. For the baseline case, computed time averaged thrust and discharge current values match laboratory measurements to within 9% and 5%, respectively. The addition of charge exchange and increase in number of particles do not influence the time averaged results significantly. However, when the plume mobility parameter is varied, the thrust and discharge current change drastically, and in a non-monotonic way. Limitations of HPHall are identified, and plans for nested channel modeling and simulation are presented.

Nomenclature

A_r, A_z, A_θ	= magnitudes of the radial, axial, and azimuthal components of $\vec{A}$
$\vec{B}$, $\vec{E}$	= magnetic and electric field vectors
d_{OC}	= outer channel diameter
e	= elementary charge
E_i	= first ionization energy
$\vec{j}_e$	= electron current density
L	= channel length
m_e	= electron mass
$\dot{m}$	= mass flow rate
$\vec{q}_e$	= thermal conduction vector
V_d	= discharge voltage
ϕ'	= normalized ion production cost
λ	= magnetic stream function
$\mu_{e,\perp}$	= cross-field electron mobility
ν_e	= total effective electron collision frequency
ν_{en}, ν_{ei}, ν_w	= frequency of electron-neutral, electron-ion and electron-wall collisions
ν_b	= electron collision frequency due to anomalous Bohm diffusion
ω_{ce}	= electron cyclotron frequency
Ω_e	= electron Hall parameter

*Graduate Student Research Assistant, Aerospace Engineering, horatiud@umich.edu.
†James E. Knott Professor, Aerospace Engineering, iainboyd@umich.edu.

I. Introduction

HALL effect thrusters (HETs) have been in development for more than 50 years, and due to their low thrust but high efficiency, they are typically used on spacecraft for stationkeeping or orbit-raising. However, recently there has been a push for higher power devices that may be used for primary propulsion (for example the Asteroid Redirect Mission[1]). An attractive way to use Hall thrusters for primary propulsion while maintaining a small footprint on the spacecraft is to nest multiple channels. This concept is demonstrated by the 10 kW class dual channel HET, dubbed "X2", developed at the Plasmadynamics and Electric Propulsion Laboratory (PEPL) at the University of Michigan. The channels can operate independently or together, increasing the throttling range for the device. Moreover, Liang[2] observed additional thrust gains due to the channel interaction. Specifically, while keeping a constant flow rate, a thrust increase between 4% and 9% (depending on the propellant mass flow rate) was recorded for dual channel operation when compared to the sum of thrust values from individual single channel tests, as demonstrated in Fig. 1a.

In order to qualify a thruster for flight, rigorous ground testing must be performed, and this is often expensive and time consuming. Moreover, facility effects[3] may influence the measurements and give unrealistic expectations compared to real performance in space. Additionally, there are still aspects of thruster operation that are not well understood, such as anomalous electron transport. Therefore, computer simulations and analytical models provide valuable insight into the development and performance of HETs.

Fife[4] developed an HET simulation tool at MIT in 1998: the axisymmetric hybrid-PIC code HPHall. The code treats heavy species (ions and neutrals) as particles, and electrons as a fluid in order to expedite computations, while reproducing the physics. An updated version of HPHall[5−8] is being used in the present study to help characterize the X2 thruster, and to understand channel interaction.

The nested channel Hall thruster modeling and simulation campaign is divided into three segments, each with its own challenges and goals:

1. independent inner channel
2. independent outer channel
3. dual channel

The first step is to simulate the independent operation of the inner channel. The research goal is to explore the capabilities of HPHall and sensitivity to numerical parameters. The next step is to simulate the outer channel independent operation. Due to code limitations, this is not possible currently, so the goal for the second stage is to update HPHall. Finally, dual channel simulations will be performed to study the channel interaction. The outer channel and dual channel simulations cannot be performed with HPHall at the present time because the quasi 1D electron model cannot function with the complicated magnetic field topology which includes opposing radial components of the magnetic field in the two channels, and a separatrix region in the plume. The radial component of the magnetic field is plotted in Fig. 1b, showing positive values in the inner channel region and negative values in the outer channel. Magnetic streamlines are also shown, and the separatrix region can be seen in the plume, between the two channels. Therefore, the current paper is focused on the independent operation of the inner channel.

The thruster operating in dual channel mode is shown in Fig. 2a, and the choice of simulation domain is illustrated in Fig. 2b. The setup is explained in Section II, results from five sets of cases are shown in Section III, conclusions are presented in Section IV, and plans for future work are outlined in Section V.

II. Simulation Setup

The thruster operating condition for the simulations is chosen based on the availability of experimental data. Since laboratory measurements for thrust, discharge current, electron temperature and plasma potential are available at $V_d = 200$ V and $\dot{m} = 75\%$ of nominal, the simulations are performed for this case.

HPHall is a serial code, and all simulations are ran in a Ubuntu 12.04 environment, on an Intel Xeon E5-1650 processor (12 cores at 3.2 GHz each). The code is compiled with GNU compilers. The magnetic field and computational mesh are illustrated in Sec.II.A, electron mobility and temperature anisotropy modeling is described in Sec. II.B, and all the other significant computational parameters and physical effects are presented in Sec. II.C.

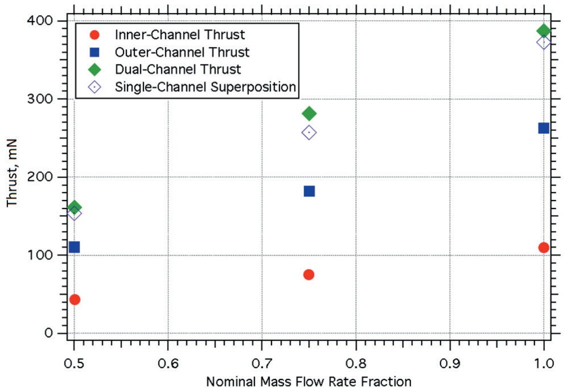

(a) Thrust gains.[2]

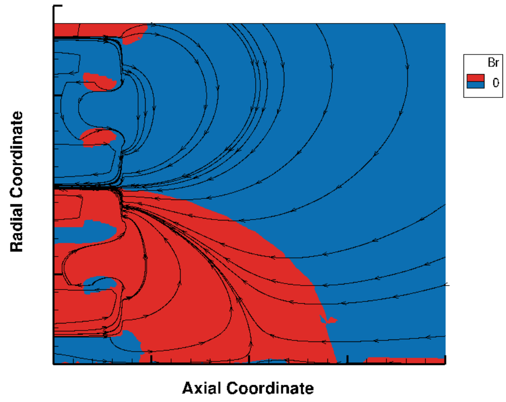

(b) Radial component of magnetic field.

Figure 1: Motivation and challenges for nested channel simulations.

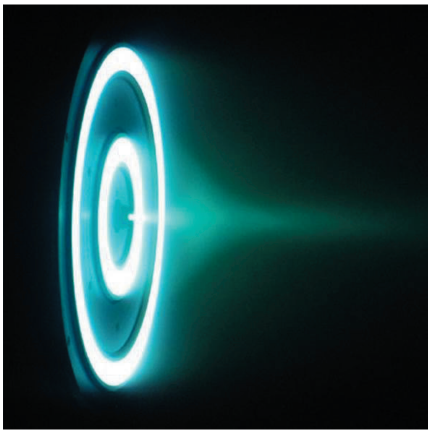

(a) Dual channel mode.[2]

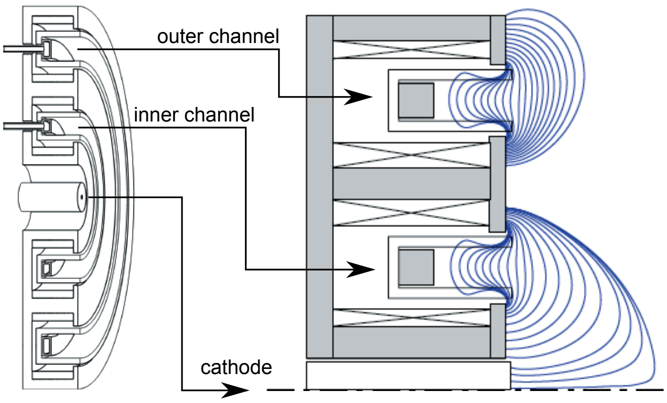

(b) Simulation setup. See Fig. 3a.

Figure 2: X2 thruster, in the laboratory, and simulation.

II.A. Magnetic Field and Mesh

The magnetic field and mesh are generated independently in the pre-processing stage, using commercial software. The magnetic field is exported from Infolytica MagNet,[9] and the mesh is built in Tecplot.[10]

Figure 3a shows the 45×30 element computational mesh. Figure 3b shows the normalized magnitude of the magnetic field, along with magnetic field lines. Note that during laboratory testing[2] the magnets were tuned for each operating point, so in order to simulate a different condition, the magnetic field input file needs to be updated.

In HPHall, the computational domain lies between the anode and cathode lambda lines, where the magnetic stream function lambda[4] is defined in Eq. 1:

$$\frac{\partial \lambda}{\partial z} = rB_r \text{ and } \frac{\partial \lambda}{\partial r} = -rB_z \tag{1}$$

The cathode potential is set at a point in the domain that lies on a lambda line which passes through the physical location of the cathode. This is the cathode lambda line. The X2 cathode is center mounted, and plasma potential data is available at the channel centerline. A value of 30 V was measured by Liang[2] with a floating emissive probe at the location indicated by a white circle in Fig. 3b. The code uses a Dirichlet boundary condition for electron temperature at the cathode location, which is set to 1 eV.

Neutral xenon gas particles are injected through the anode at a flow rate of 7×10^{-6} kg/s with a temperature of 750 K[11] and a Mach number of 0. Similarly, Xe is added at the cathode location at a rate that is 10% of the anode flow, as reported by Liang.[2] Data for the X2 cathode was not available, but based on values used by Choi[12] for an H6 thruster cathode, neutrals are injected with a temperature of 823 K and Mach number of 0.6.

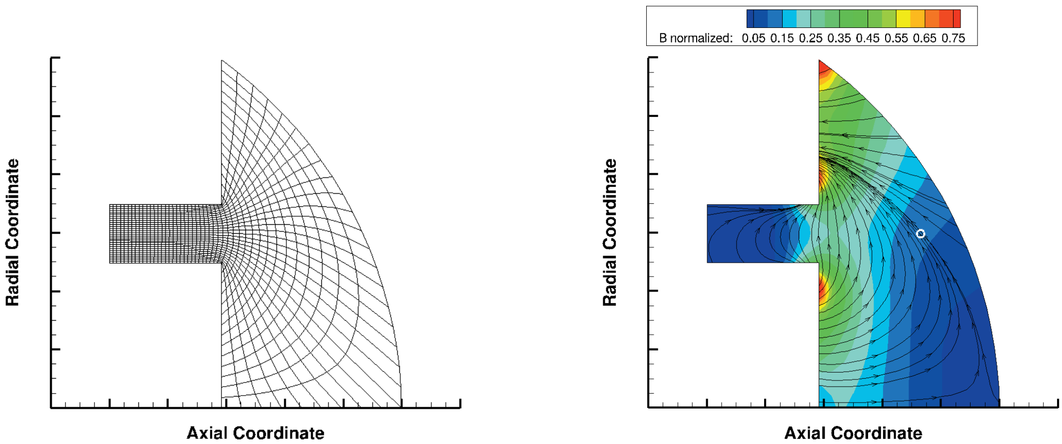

(a) Computational mesh.

(b) Magnetic field.

Figure 3: HPHall inputs generated with pre-processing software.

II.B. Electron Handling

II.B.1. Electron Mobility

The version of HPHall used in this study employs a three-region mobility model, as described by Hofer.[8] This approach allows for better tuning of the mobility in the discharge channel, exit plane and plume regions. The cross field mobility is defined as:

$$\mu_{e,\perp} = \frac{e}{\nu_e m_e}\left(\frac{1}{1+\Omega_e^2}\right) \tag{2}$$

The total effective electron collision frequency is computed from:

$$\nu_e = \nu_{en} + \nu_{ei} + \nu_w + \nu_b \tag{3}$$

Anomalous transport is modeled by including an adjustable parameter, α:

$$\nu_b = \frac{1}{16}\alpha\omega_{ce} \tag{4}$$

where classical Bohm diffusion is recovered by setting $\alpha = 1$.

The three regions must be defined in relation to the thruster geometry, and values for the adjustable parameter α in each region must be set. Selecting these values involves an iterative procedure to ensure agreement with experimental data. Hofer[8] approached this problem by evaluating the Hall parameter from experimentally measured data, as shown in Fig. 4. This curve suggests how the three regions should be defined. In order to optimize the mobility coefficients, the plume mobility is first set to $\alpha = 1$, while the channel and exit coefficients are adjusted to match the discharge current. If necessary, the plume coefficient may then be adjusted to further improve the agreement with measurements.

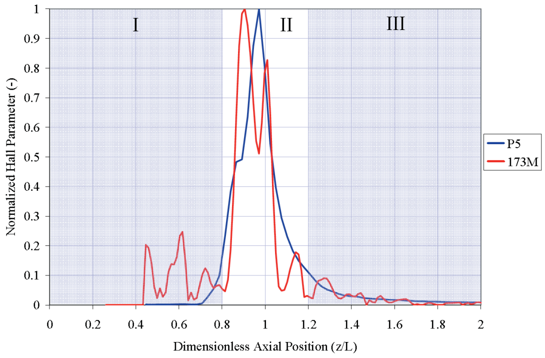

Figure 4: Hall parameter versus axial position computed from experimental data by Hofer.[8] The discharge channel exit plane is located at $z/L = 1$.

The simulations presented here follow a similar procedure. However, azimuthal and perpendicular values of current density[13] are not available, and therefore it is not possible to evaluate the Hall parameter based on measurements. Hence, the locations of the mobility regions are determined after several iterations. The dimensionless positions (axial coordinate over channel length) described by Hofer[8] are used as a starting point. Adjustments are made, and final region boundaries are chosen based on discharge current matching. The mobility coefficients are selected similarly, and further discussion on this topic is provided in Section III.D.

The final choices of Bohm region boundaries and coefficient values for the baseline case are summarized in Table 1. An interpolation is performed in the transition region to provide a smooth profile between mobility regions, but an abrupt transition may also be implemented, as shown in the second row.

Table 1: Mobility parameters for the baseline case.

Region	**Start transition (z/L)**	**End transition (z/L)**	**Coefficient**
channel	0.8	0.8	0.14
exit	0.8	1.13	0.07
plume	1.13	1.27	1.0

II.B.2. Temperature Anisotropy

Although the electron mobility has the most significant effect on thrust results, electron temperature anisotropy can also have a large influence. In HPHall, Fife[4] uses a quasi 1D electron model, which assumes that the electron temperature is constant along magnetic field lines, as shown in Eq. 5.

$$T_e = T_e(\lambda) \tag{5}$$

Across field lines, the electron temperature is computed from Eq. 6.

$$\frac{\partial}{\partial t}\left(\frac{3}{2}n_e k T_e\right) + \nabla \cdot \left(\frac{5}{2}n_e k T_e \vec{u}_e + \vec{q}_e\right) = S_h - S_i \tag{6}$$

where

$$\begin{aligned} S_h &= \vec{j}_e \cdot \vec{E} \\ S_i &= \dot{n}_e \varphi' E_i \end{aligned}$$

Fife's thesis[4] provides further details regarding the calculation of the volumetric electron energy loss, S_i.

$$T_e^{corrected} = \frac{T_{e,\parallel}}{T_{e,\perp}} T_e^{uncorrected} \tag{7}$$

Anisotropy is accounted for by including a correction for the electron temperature values used in the wall loss term, and Bohm speed computation, as shown in Eq. 7. A constant ratio of parallel to perpendicular temperatures is used throughout the entire domain, and for the simulations presented here the value is 0.86. This parameter is studied in Section III.E.

II.C. Additional Parameters and Physics

The X2 thruster was tested in the Large Vacuum Test Facility (LVTF) at PEPL, and for the conditions of interest, Liang[2] reported a facility backpressure of 1.5×10^{-5} Torr. The backpressure effects are included in the simulation via neutral Xe injection at the outflow boundary of the domain at an assumed temperature of 300 K.

For the present simulations, no significant changes are observed when compared to a pure vacuum test case. However, a 17.3% increase in thrust and 17.8% increase in discharge voltage are observed for a simulation run at 3.11×10^{-4} Torr, 20 times the LVTF backpressure. The value corresponds to a neutral number density of 10^{19} m^{-3} which is on the order of the observed neutral density inside the thruster for the baseline simulation. This choice of backpressure is made to replicate neutral ingestion and observe changes in thrust and discharge current. The simulation outputs show a significant response, thus, in order to verify the thrust improvements observed by Liang in dual channel mode, it is crucial to include backpressure in the simulation.

The effect of charge exchange (CEX) collisions between ions and neutrals is studied. The implementation used in HPHall is that described by Parra.[15]

In HPHall, the heavy species timestep is frozen while electron computations take place. Thus, two different time increments are used. For stability, the electron timestep is set to a value of O(10^3) smaller than the heavy species step. The timestep used for ions and neutrals, along with the spatial grid size are chosen to resolve gradients in the simulation.

The heavy species present in the simulations are xenon neutrals, singly charged, and doubly charged xenon ions. Smith[16] has added the capability to include triply charged ions, however it is not used for these simulations.

The total number of particles in the simulation varies both in time, and between the different cases studied. A comparison between the baseline and CEX simulations is reported in Section III.B, and the effects of an increase in number of particles are investigated in Section III.C.

The wall temperature value inside the channel is estimated based on thermocouple measurements performed on a SPT-100 thruster operating at similar power levels.[11]

HPHall is run in three different stages. First, the domain is populated with neutrals, and this stage takes 20,000 timesteps. Next, ion particles are added for another 20,000 timesteps. Finally, the ion-neutral and ion-ion collisions are activated, and this stage takes 80,000 timesteps (4 ms of physical time). Identical parameters are used for all three stages, with the exception of the electron time step which is adjusted to ensure code stability. Table 2 summarizes the input parameter values.

Table 2: Input parameters.

Propellant gas	Xe
Propellant flow rate at anode	7×10^{-6} kg/s
Cathode flow rate	7×10^{-7} kg/s
Facility backpressure	1.5×10^{-5} Torr
Discharge voltage	200 V
Channel wall temperature	812 K
Heavy particle timestep	5×10^{-8} s
Electron timestep	5×10^{-11} s
Total simulation time	4 ms

III. Results

Several simulation parameters and physical effects are studied. First, a baseline case is presented in Sec. III.A. Next, CEX collisions are added and the observed differences are shown in Sec. III.B. Further, two simulations similar to the baseline are run with higher total numbers of particles in Sec. III.C. Sensitivity to the mobility coefficients is explored in Sec. III.D. Finally, the effects of electron temperature anisotropy are investigated in Sec. III.E. Unless otherwise noted, only one parameter is varied, while the others are kept the same as in the baseline case.

III.A. Baseline

Figure 5 shows contour maps of the number density of xenon neutral atoms (Fig. 5a) and singly charged xenon ions (Fig. 5b). Streamtraces are shown in both figures, and particles generally travel from higher to lower density regions. The two high density areas seen in the neutral plot correspond to the anode and cathode particle injection locations, while the high density area of the ion map is the ionization region.

Figures 6 and 7 illustrate the plasma potential and electron temperature from the simulation and show how these values compare to measurements[2] performed along the thruster centerline. The axial coordinate in the line plots is normalized with respect to the outer channel diameter of the X2. The normalized axial coordinate of 0 is located at the thruster exit. The simulation results are shown as the red line and the green squares indicate experimental values recorded during independent inner channel operation (IC).

A contour map of plasma potential is shown in Fig. 6a. The potential drops from 200 V to 30 V, as expected for the anode and cathode parameters used. As shown in Fig. 6b, the decrease in potential matches the measurements very well. Figure 7a illustrates the distribution of electron temperature in the domain, with a peak near the thruster exit plane. The comparison with measurements shows that the peak is 2 eV higher and has a broader distribution in the simulation.

III.B. Effects of Charge Exchange

The plots shown for the baseline case in Section III.A remain largely unchanged after CEX collisions are added. This section will focus only on the differences that are observed.

CEX has an effect on neutral and ion velocities. Figure 8 compares the ion velocity in the axial direction and it can be seen that the baseline case (Fig. 8a) shows a larger peak region than seen in the CEX simulation (Fig. 8b). A similar effect is observed for the radial ion velocity, in Fig. 9. However, the trend is reversed when considering the axial neutral velocity shown in Fig. 10. A region of high axial neutral velocity can be observed in the CEX results (Fig. 10b) which is not present in the baseline case (Fig. 10a). The addition of charge exchange appears to not have a significant effect on the radial component of the neutral velocity as seen in Fig. 11.

The addition of charge exchange also changes the time dependent simulation behavior. Figure 12 indicates that discharge current oscillations have a lower amplitude in the CEX simulation, and they do not exhibit a decaying behavior as seen in the initial 0.5 ms transient of Fig. 12a.

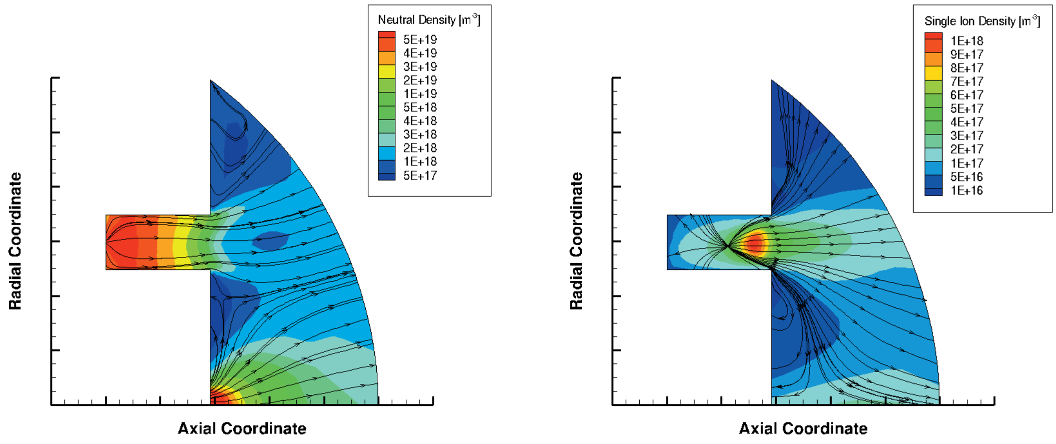

(a) Xe neutral atoms.

(b) Xe^+ singly charged ions.

Figure 5: Density contour maps.

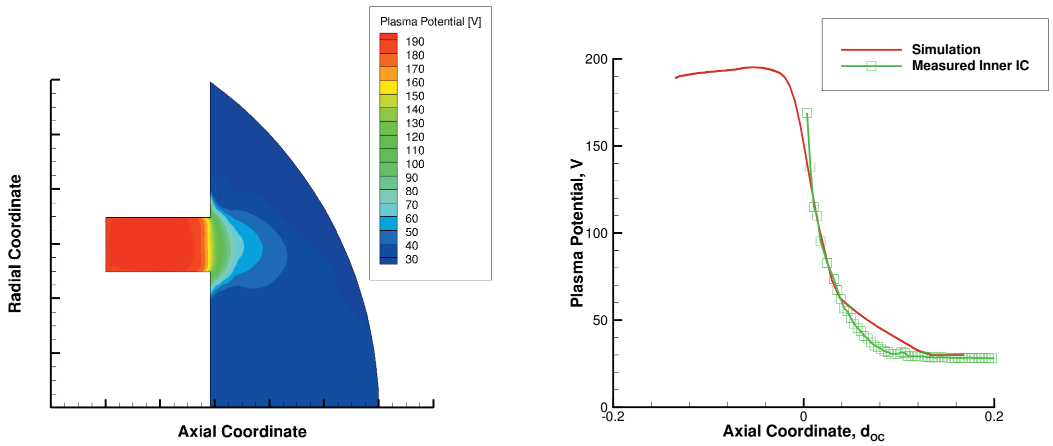

(a) Entire domain.

(b) Along inner channel centerline.

Figure 6: Plasma potential.

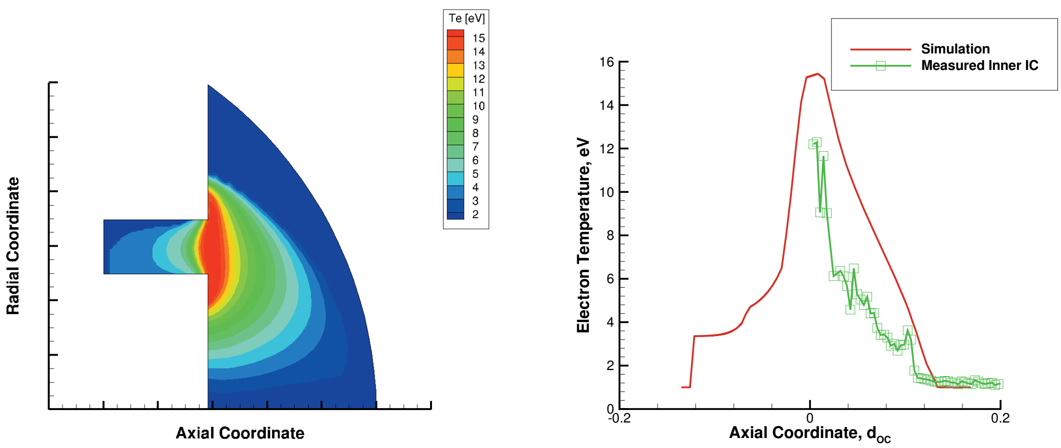

(a) Entire domain.

(b) Along inner channel centerline.

Figure 7: Electron temperature.

The total number of neutral particles in the simulation reaches a saturation level in both cases, as shown in Fig. 13. However, this value is an order of magnitude higher in the CEX (Fig. 13b) case than the baseline (Fig. 13a). Since the dynamic range is significantly larger, CEX produces a much smoother curve.

The total number of ion particles in the simulation fluctuates differently for the baseline and CEX cases, as seen in Fig. 14. The baseline Fig. 14a shows an initial increase in the mean value, while the CEX plot shows the opposite in Fig. 14b.

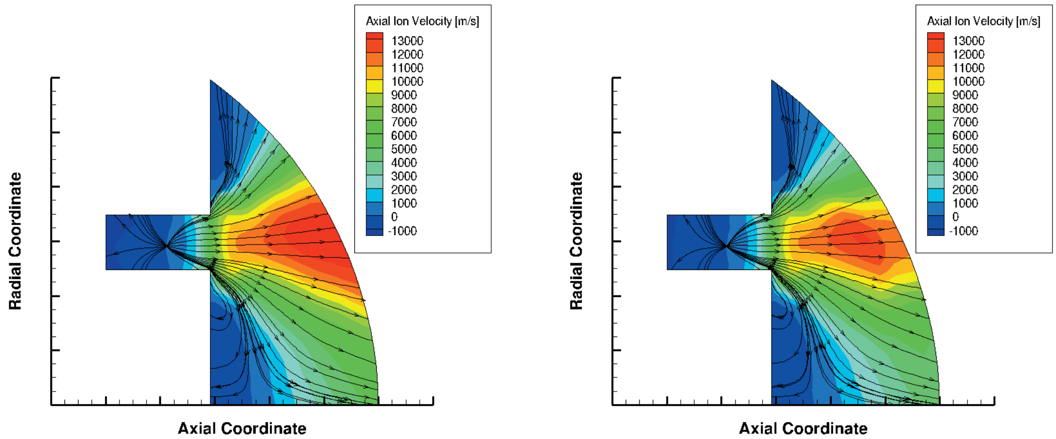

(a) Baseline. (b) With CEX.

Figure 8: Ion velocity in the axial direction.

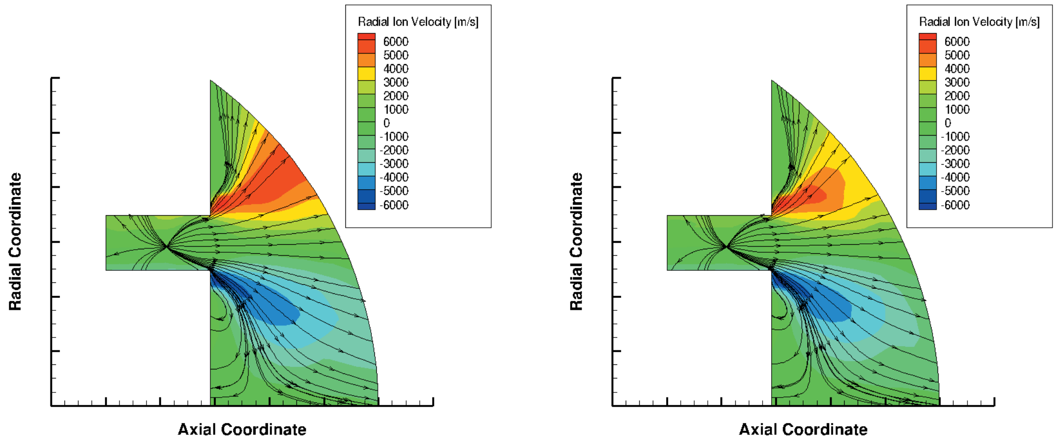

(a) Baseline. (b) With CEX.

Figure 9: Ion velocity in the radial direction.

III.C. Increased Number of Particles

The different time dependent behavior between the baseline case and CEX simulation may be due to the large difference in the number of particles used in the two cases. Therefore, the baseline case simulation is run again, first with six (6x) and then with ten times (10x) more particles than the initial case. The time evolution of discharge current is shown in Fig. 15. Both 6x (Fig. 15a) and 10x (Fig. 15b) cases produce a lower noise level when compared to the baseline and CEX cases from Fig. 12.

The total number of particles is compared for all four cases in Fig. 16. Figure 16a illustrates the variation in the total number of ions. The baseline and CEX curves are on the same order of magnitude, while for 6x and 10x the number of ions is approximately 6 and 10 times larger, respectively. Figure 16b shows how

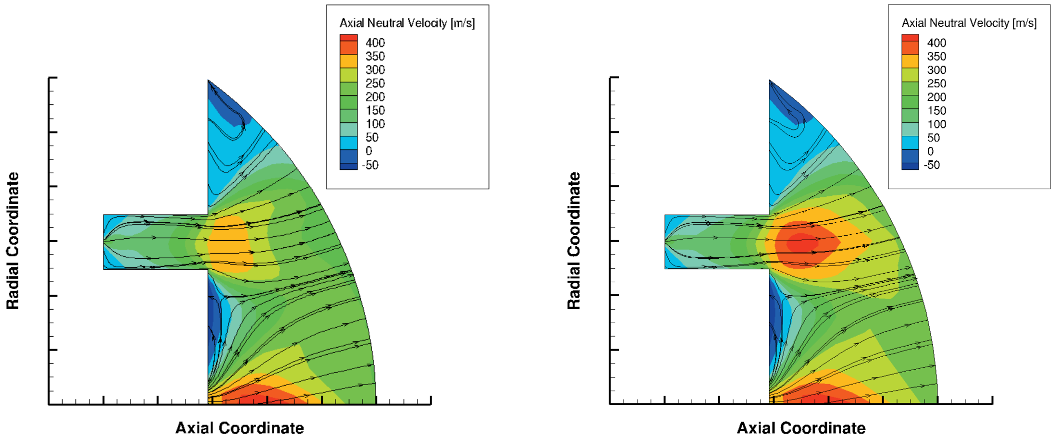

(a) Baseline.　　(b) With CEX.

Figure 10: Neutral velocity in the axial direction.

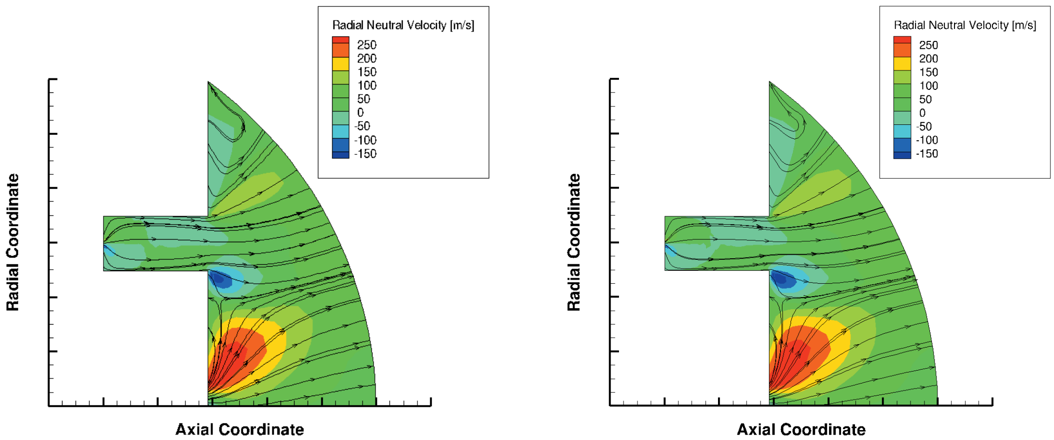

(a) Baseline.　　(b) With CEX.

Figure 11: Neutral velocity in the radial direction.

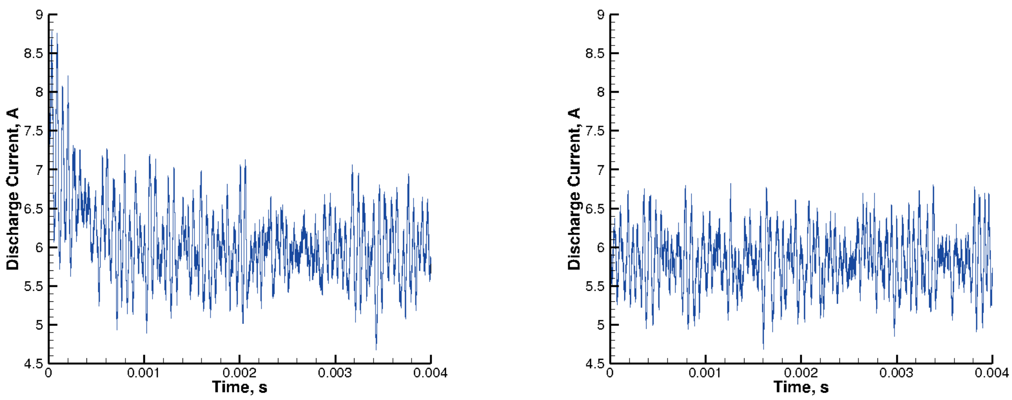

(a) Baseline.　　(b) With CEX.

Figure 12: Time evolution of discharge current.

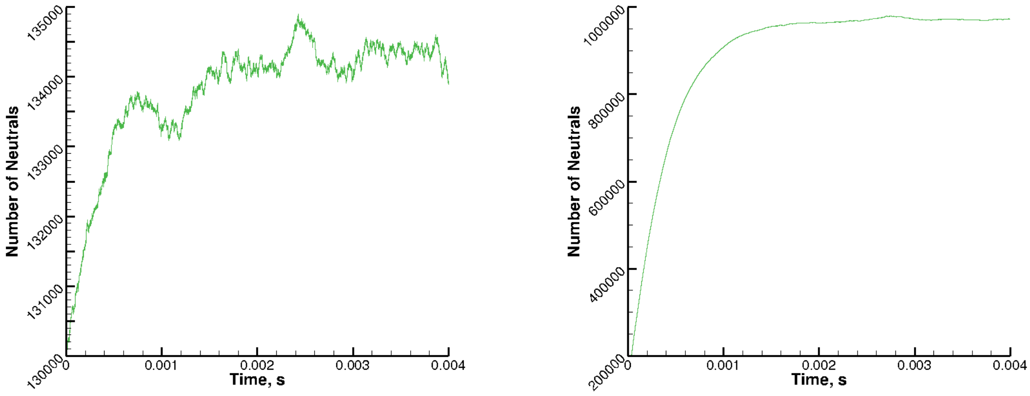

(a) Baseline. (b) With CEX.

Figure 13: Time evolution of the total number of neutral particles.

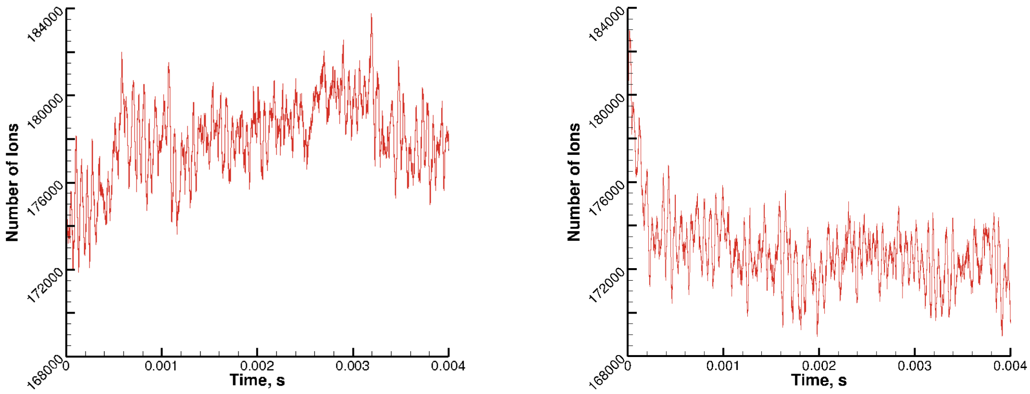

(a) Baseline. (b) With CEX.

Figure 14: Time evolution of the total number of ion particles.

the total number of neutrals changes in time. All the baseline cases display a similar, and roughly constant behavior, with 6x and 10x cases producing 6 and 10 times more particles respectively than the baseline. The number of ions in the CEX case starts at a similar value to the baseline, but keeps increasing for the first 0.0011 s until it reaches a steady state at approximately 960,000 particles.

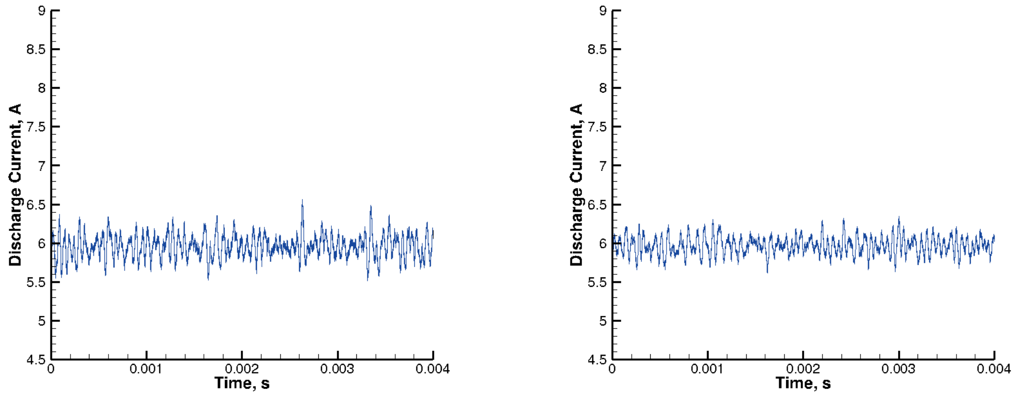

(a) 6 times more particles. (b) 10 times more particles.

Figure 15: Time dependent discharge current. Compare to Fig. 12.

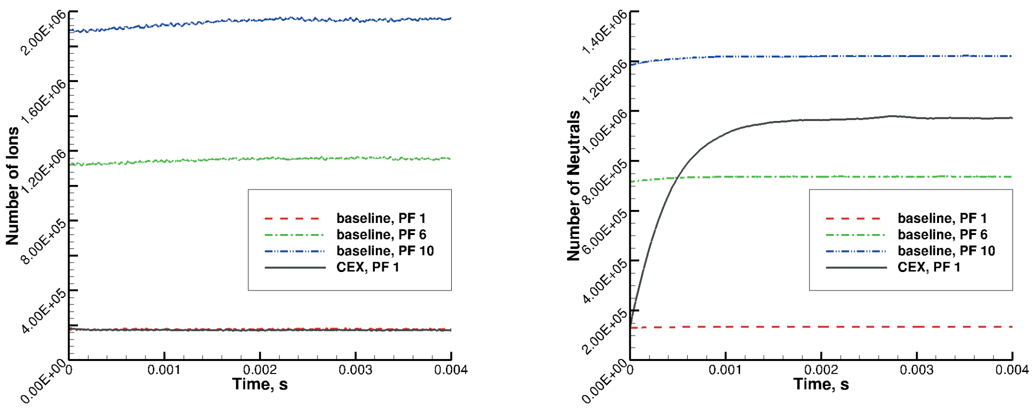

(a) Ions. (b) Neutrals.

Figure 16: Comparison of total number of particles. The baseline and CEX cases use the same data as shown in Figs. 13 and 14.

Table 3 provides a summary of time averaged results from the four simulations, as well as laboratory data. The values shown in the last column are obtained from Liang's[2] measurements. Although discharge current data was not reported directly, it was extracted from anode efficiency values provided in Liang's thesis. Note that the run time shown in the last column includes all three stages of the HPHall simulation.

The CEX case shows a decrease of 2.7 mN in total thrust from the baseline case. The time averaged values of currents also decreased by: 0.05 A for electrons, 0.18 A for singly charged ions and 0.026 A for doubly charged ions. However, the run time increased by approximately 17 hours. Overall, the addition of CEX improved agreement with experiment for the total discharge current, but reduced it for thrust.

The large number of particle simulations 6x and 10x agree very closely to each other for all observed quantities, so the baseline is only compared to the 6x case. A 1.4 mN decrease in thrust and 0.12 A decrease in total discharge current are observed. The electron current is 0.04 A lower, and singly and doubly charged ion currents are 0.07 A and 0.019 A lower, respectively. These simulations are significantly more expensive

Table 3: Time averaged results.

Case	Thrust (mN)	Total discharge current (A)	Electron current (A)	Xe^{+1} current (A)	Xe^{+2} current (A)	run time (hh:mm:ss)
baseline	81.0	6.08	1.56	4.09	0.434	09:39:23
PF 6	79.6	5.96	1.52	4.02	0.415	50:42:21
PF 10	79.8	5.97	1.52	4.03	0.415	82:11:04
with CEX	78.3	5.83	1.51	3.91	0.408	28:22:02
measured	92.0 ± 3.00	5.56 - 5.79	-	-	-	N/A

than the baseline case: the 6x case runs 5 times longer, while the 10x case runs 8 times longer.

III.D. Electron Mobility Coefficients

As described in Section II.B.1, the mobility coefficients are selected through an iterative procedure to improve the match between computed discharge current and the measured value, which lies between 5.56 and 5.79 A.[2] Sections III.D.1 and III.D.2 explore the variation in current and thrust with changes of the channel exit and plume coefficients, respectively.

III.D.1. Channel Exit Region

Figure 17b shows how time averaged quantities vary with the choice of mobility coefficient for the channel exit region. Both the discharge current (Fig. 17a) and thrust (Fig. 17b) increase with higher values of the mobility parameter. While the discharge current reaches the measured value for $\alpha = 0.065$, at this point the thrust is only 77.2 mN, giving a 13.4 % error compared to the measured 92 ± 3 mN. Further increasing the mobility parameter brings the computed thrust value higher, but it diminishes the agreement for discharge current. A compromise is made between matching the measurements for thrust and those for discharge current, and the mobility coefficient value of $\alpha = 0.07$ is chosen since it produces errors below 10% for both parameters.

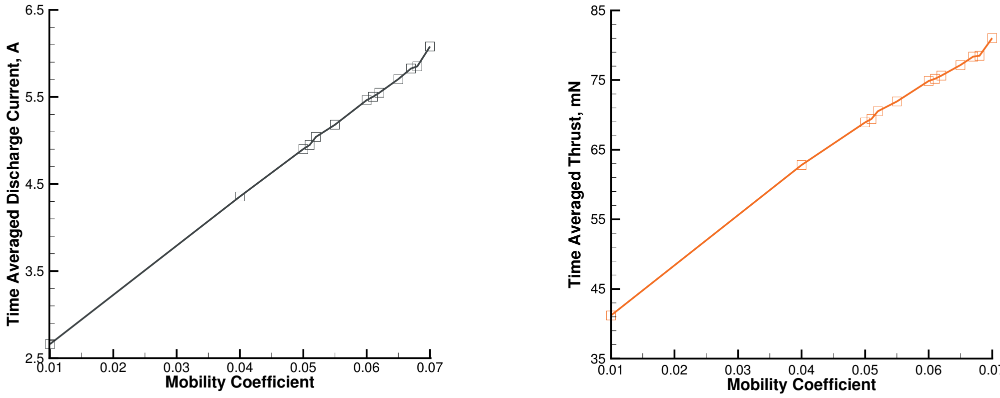

(a) Discharge current.

(b) Thrust.

Figure 17: Variation of time averaged quantities with mobility coefficient for the channel exit region (baseline). This corresponds to region II in Fig. 4.

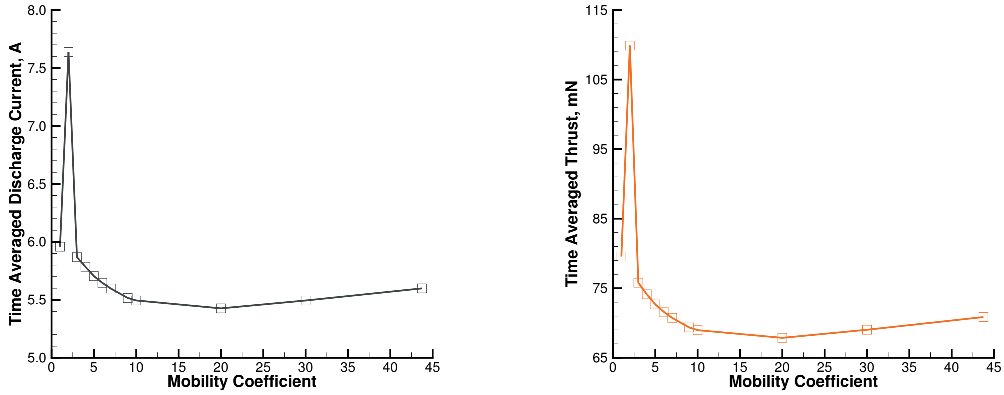

(a) Discharge current.

(b) Thrust.

Figure 18: Variation of time averaged quantities with mobility coefficient for the plume region (6x). This corresponds to region III in Fig. 4.

III.D.2. Plume Region

It is observed that the time averaged discharge current and thrust do not vary monotonically with the plume mobility coefficient, unlike the channel exit coefficient. Therefore the variation study of these quantities is performed at a larger particle factor (6x), to minimize the effects of noise. Time averaged quantities are observed for coefficient values ranging between $\alpha = 1$ (classical Bohm mobility) and $\alpha = 43.75$. Discharge current is shown in Fig. 18a and thrust in Fig. 18b. The behavior of both quantities is similar, reaching the same maximum and minimum points. A coefficient value of $\alpha = 2$ produces a sharp increase in time averaged values: 30 mN (38.1%) for thrust and 1.68 A (28.2 %) for discharge current compared to $\alpha = 1$. Increasing the coefficient between $\alpha = 2$ and $\alpha = 10$ decreases the time averaged values, but the large coefficient value of $\alpha = 43.75$ produces an increase in thrust and discharge current. Since the plume coefficient does not yield a predictable behavior for the time averaged quantities, the initial value of $\alpha = 1$ is retained, pending future investigation.

III.E. Electron Temperature Anisotropy

Hara[14] suggests that temperature anisotropy may be accounted for by including the effects of azimuthal velocity in the energy balance, as shown in Eq. 8.

$$\epsilon = \frac{3}{2}T_e + KE_\theta = \frac{3}{2}T_e + \frac{\frac{1}{2}m_e v_\theta^2}{e} \tag{8}$$

The azimuthal velocity is computed from the $E \times B$ drift, and using the axial-radial values available from HPHall it may be written as in Eq. 9.

$$v_\theta = \frac{E_z B_r - E_r B_z}{B_r^2 + B_z^2} \tag{9}$$

Next, the anisotropy ratio may be computed as the ratio of the temperature derived from Eq. 8, and the actual value computed in the code. Based on this formulation, a map of effective temperature ratio parameter is constructed for the baseline case. Figure 19 shows that the electron temperature anisotropy ratio varies throughout the domain. In the region of high electron temperature, the computed ratio is between 0.89 and 0.95, compared to the 0.86 value that is used in the simulation. Therefore in the future a dynamic way of computing the temperature ratio should be implemented, to account for the gradients observed in Fig. 19.

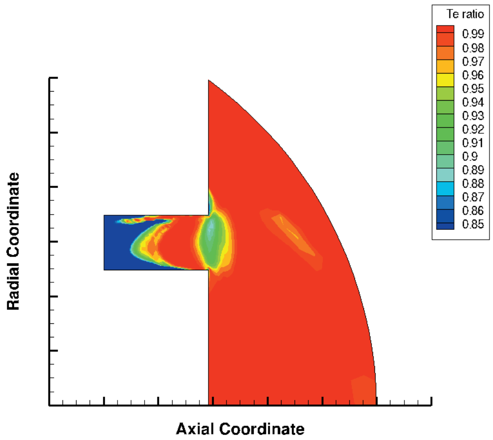

Figure 19: Electron temperature anisotropy ratio.

IV. Conclusion

A first step in the simulation of a nested channel Hall effect thruster was presented. The numerical capabilities of HPHall were explored by including cathode neutral flow, neutral backpressure, observing simulation sensitivity to the mobility parameters, investigating the effects of charge exchange and analyzing the electron temperature anisotropy ratio.

The baseline case matched time averaged thrust and discharge current measurements to within 9% and 5%, respectively. In previous simulations,[19] thrust has been matched to within the experimental error of ±3 mN. However, simultaneously matching the discharge current value is challenging because thrust tends to be lower than the measured value, while discharge current is higher, yet higher thrust simulations tend to have even higher discharge current values. This study shows the closest simultaneous agreement to X2 experimental data for both quantities, to date.

The inclusion of charge exchange collisions lowered the thrust and time averaged discharge current by 3.33% and 4.11%, respectively. The decrease occurred because a larger population of slow ions reached the boundary domain while faster neutrals remained near the channel exit. The CEX simulation results agreed with thrust measurements to within 14% and time averaged discharge current to within 0.7%. The current fractions for the baseline case were 0.904 for singly charged xenon ions and 0.095 for doubly charged ions. The addition of charge exchange did not make a significant impact on the fractions, which were 0.905 and 0.094, respectively. However, the charge exchange simulation took approximately 3 times longer than the baseline case to complete, so the run time is expected to increase significantly for a larger numbers of particles.

Differences in the time dependent evolution of discharge current and number of neutral particles observed between the baseline and CEX simulation prompted new simulations with a larger number of particles: six and ten times more than the baseline. The two cases agree well with each other. The 6x case shows a 1.7% decrease in thrust and 1.97% decrease in total discharge current when compared to the baseline case. The electron current is (1%) lower, and singly and doubly charged ion currents are 1.7% and 4.4% lower, respectively. The large particle factor cases were 5 (6x) and 8 (10x) times more expensive than the baseline simulation.

The HPHall time averaged outputs (thrust and discharge voltage) showed significant sensitivity to the mobility parameters. The addition of CEX collisions, and changes in number of particles had less of an effect on the simulation results, and major differences were observed only in the transient behavior. Additionally, it was shown that the implementation of a constant electron temperature anisotropy ratio throughout the entire domain should be reconsidered.

The next step is to simulate the outer channel independent operation, followed by a dual channel mode simulation. However, the quasi 1D thermalized potential electron model used in HPHall is inadequate for such cases due to the complex magnetic field topology. Therefore, a two dimensional (axial-radial) electron model is currently being developed and will be included in HPHall in the near future.

V. Future Work

Fife[4] used a thermalized potential approximation giving a quasi 1D electron model: the electron temperature is considered constant along magnetic lines of force. Geng and Keidar[17] have made a preliminary investigation into the validity of this assumption for HETs, and concluded that it may only be used for very simple field topologies with no strong gradients in number density or electron temperature. Moreover, the HPHall computational domain is only defined between an anode field line and a cathode field line, so detailed plume analysis is impossible.

In order to simulate more complicated field geometries, JPL moved away from the hybrid PIC approach to a multi-fluid model developed by Mikellides.[18] This approach reduces the statistical noise produced by the PIC algorithm and allows simulation of complicated magnetic field topologies. However, due to the use of a fluid model for the heavy species, non-Maxwellian velocity distribution functions (VDFs) cannot be resolved. Therefore, the hybrid-PIC approach remains a useful alternative simulation tool.

Before nested channel devices can be simulated with HPHall, the electron model will need to be replaced by a 2D axial-radial version which does not rely on the thermalized potential assumption. In addition to a new momentum equation, the electron temperature computation may be improved by following Hara's[14] approach to yield a self-consistent value of the electron temperature ratio which does not have to be predetermined through iteration.

In summary, the following steps will be taken to continue the modeling and simulation work for nested channel Hall thrusters:

1. generation of a Hall parameter map from experimental measurements
2. implementation of a self-consistent value of the electron temperature ratio
3. update the quasi 1D electron model to a 2D axial-radial version

Acknowledgments

This work was supported by a NASA Space Technology Research Fellowship, (grant number: NNX13AL51H), under Mr. G. Soulas' guidance.

H. C. Dragnea would like to thank M. Choi for providing neutral cathode flow data, M. Georgin for his assistance in preparing the MagNet maps, S. J. Hall for facilitating access to additional data, and verification of the magnetic field, Dr. K. Hara for the discussion on electron temperature anisotropy, Dr. R. Liang for providing clarification for the X2 data, A. Raisanen for providing feedback that improved the clarity of figures and B. D. Smith for sharing some of his experience with running HPHall simulations.

References

[1]Brophy, J.R., "Technology for a Robotic Asteroid Redirect Mission", *2014 IEEE Aerospace Conference*, DOI:10.1109/AERO.2014.6836392, Big Sky, MT, March 1-8, 2014

[2]Liang, R, "The Combination of Two Concentric Discharge Channels into a Nested Hall-Effect Thruster," Ph.D. Dissertation, Dept. of Aerospace Engineering, University of Michigan, Ann Arbor, MI, 2013.

[3]Byers, D., and Dankanich, J.W., "A Reveiew of Facility Effects on Hall Effect Thrusters", *31st International Electric Propulsion Conference*, IEPC-2009- 076, Ann Arbor, MI, September 20-24, 2009

[4]Fife, J.M., "Hybrid-PIC Modeling and Electrostatic Probe Survey of Hall Thrusters," Ph.D. Dissertation, Dept. of Aeronautics and Astronautics, Massachusetts Institute of Technology, Cambridge, MA, 1998.

[5]Hofer, R.R., Mikellides, I.G., Katz, I., and Goebel, D.M., "BPT-4000 Hall Thruster Discharge Chamber Erosion Model Comparison with Qualification Life Test Data", *30th International Electric Propulsion Conference*, IEPC-2007-267, Florence, Italy, September 17 - 20, 2007.

[6]Gamero-Castano, M. and Katz, I., "Estimation of Hall Thruster Erosion Using HPHall", *29th International Electric Propulsion Conference*, IEPC-2005-303, Princeton University, Princeton, October 31 - November 4, 2005.

[7]Hofer, R.R., Mikellides, I.G., Katz, I., and Goebel, D.M., "Wall Sheath and Electron Mobility Modeling in Hybrid-PIC Hall Thruster Simulations", *43rd AIAA/ASME/ SAE/ASEE Joint Propulsion Conference*, AIAA 2007-5267, Cincinnati, OH, July 8 - 11, 2007.

[8]Hofer, R. R., et al., "Efficacy of Electron Mobility Models in Hybrid-PIC Hall Thruster Simulations," *AIAA/ASME/SAE/ASEE Joint Propulsion Conference & Exhibit*, AIAA 2008-4924, Hartford, CT, July 21-23, 2008.

[9]MagNet, Infolytica Corporation, Software Package, Ver.7.3.0.146, Montréal, Québec, Canada.

[10]Tecplot 360, Tecplot, Inc., Software Package, Ver. 2013R1, Bellevue, WA.

[11]Archipov, B. A., Krochak, L. Z., and Maslennikov, N. A., "Thermal Design of the Electric Propulsion System Components:

Numerical Simulations ," *AIAA/ASME/SAE/ASEE Joint Propulsion Conference & Exhibit*, AIAA 1998-3489, Cleveland, OH, July 13-15, 1998.

[12]Choi, M., and Boyd, I. D.,"Numerical Simulation of the Cathode Plume of a Hall Thruster," *AIAA/ASME/SAE/ASEE Joint Propulsion Conference & Exhibit*, AIAA 2014-3427, Cleveland, OH, July 28-30, 2014.

[13]Haas, J. M., "Low-perturbation Interrogation of the Internal and Near-field Plasma Structure of a Hall Thruster Using a High-speed Probe Positioning System," Ph.D. Dissertation, Dept. of Aerospace Engineering, University of Michigan, Ann Arbor, MI, 2001.

[14]Hara, K., Sekerak, M. J., Boyd, I. D., and , Gallimore, A.D. "Mode transition of a Hall thruster discharge plasma," *Journal of Applied Physics*, Vol. 115, 2014, DOI: 10.1063/1.4879896.

[15]Parra, F. I., Ahedo, E., Fife, J. M., and , Martinez-Sánchez, M. "A two-dimensional hybrid model of the Hall thruster discharge," *Journal of Applied Physics*, Vol. 100, 2006, DOI: 10.1063/1.2219165.

[16]Smith, B. D., Boyd, I. D., and Kamhawi, H.,"Influence of Triply-Charged Ions and Ionization Cross-Sections in a Hybrid-PIC Model of a Hall Thruster Discharge," *AIAA/ASME/SAE/ASEE Joint Propulsion Conference & Exhibit*, AIAA 2014-3429, Cleveland, OH, July 28-30, 2014.

[17]Geng, J., Brieda, L., Rose, L., and Keidar, M. "On Applicability of the "Thermalized Potential" Solver in Simulations of the Plasma Flow in Hall Thrusters," *Journal of Applied Physics*, Vol. 114, 2013, DOI: 10.1063/1.4821018.

[18]Mikellides, I.G., Katz, I., Hofer, R. R., and Goebel, D. M. "Hall-Effect Thruster Simulations with 2-D Electron Transport and Hydrodynamic Ions", *31st International Electric Propulsion Conference*, IEPC-09-114, Ann Arbor, MI, September 20-24, 2009

[19]Dragnea, H. C., Boyd, I. D., Hall, S. J., and Gallimore, A. D.,"Preliminary Results and Future Goals for a Simultaneous Characterization of a Nested-channel Hall Thruster in Experiment and Simulation," *The* 20^{th} *Advanced Space Propulsion Workshop*, Ohio Aerospace Institute, Cleveland, OH, November 17-19, 2014.